Author's response to:
RC#1
https://doi.org/10.5194/egusphere-2025-4517-RC1

Anton Kötsche[1], Maximilian Maahn[1], Veronika Ettrichrätz[1], and Heike Kalesse-Los[1]

[1]Leipzig Institute for Meteorology (LIM), Leipzig University, Leipzig, Germany

Correspondence: anton.koetsche@uni-leipzig.de

Summary of main changes of the manuscript:

- Added rationale to the empirical δ retrieval in Section 2.1.2 Polarimetric radar data, since our approach to removing δ from KDP is not published in another study (to our knowledge there is no other literature available that discusses the removal of δ in snow at W-band). We provide some plots of cases with δ for the reviewer to evaluate the δ removal method.
- Added new section (2.6 The turbulent layer) to explain turbulent layer formation behind Gothic Mountain based on a representative case study, since a more detailed description of the formation mechanism was requested by reviewer 2.
- Removed Sect 3.1 Case Study on February 21, 2023 because of the concerns of reviewer 2 regarding the influence of SIP not related to the turbulent layer and the close proximity of the cloud top to the turbulent layer, resulting in increased influence of INP.
- Small changes in the schematic figure requested by reviewer 1 (Fig. 11 in new manuscript)
- Improvement of the map in the appendix based on remarks by reviewer 1 (B1)

Response to RC#1:

General comment #1: Figure 12

New Figure 12: thanks for adding this figure, quite helpful. But I have some questions/suggestions

Please see the updated figure (3) on one of the following pages, we tried to incorporate your helpful suggestions as best as possible.

(a) *I would recommend to use the same number of variables in the same order for all quadrants, to ease the comparison from one to the other.* We tried to adapt the order of the variables. However, we only display variables that would significantly changer during the respective process, also showing the variables that don't change would use to much space.

(b) *I would start by Ze and MDV, which gradients are defining the quadrants.* Done

(c) *Similarly for Quadrant IV: Ze and MDV should only be decreasing. If you want to indicate of the gradient is small or large, please find another visual "marker"* Riming increases Ze (upper row of quadrant IV) and sublimation decreases it (lower row of quadrant IV). The net change visible as Ze gradient therefore depends on the impact of the individual processes taking place in the turbulent layer.

(d) *We cannot know if the VISSS derived variables increase or decrease in space, only if they are rather small or large. So here as well use another visual marker. Or do you refer to changes in time?* We refer to the suspected change of the VISSS variable due to the process. Aggregation for example, is known to increases complexity C and D32. This is what we also wrote in the caption of the figure: "VISSS variables (Ntot, C, D32, M) are measured below the turbulent layer. Their change due to the microphysical process is suspected based on the change of particle and PSD properties. If a variable is not depicted, no clear trend can be derived."

General comment #2: Supersaturation

I asked a question about supersaturation with respect to liquid water (to form dendrites) and you answered with a figure about supersaturation with respect to ice... Please update.

Excuse the confusion, we assumed you meant supersaturation with respect to ice, since dendrites grow by depositional growth in the dendritic growth layer and hence require supersaturation with respect to ice. It's not physically impossible to momentarily have supersaturation w.r.t. water at these temperatures but once ice crystals are present in meaningful numbers, the Bergeron–Findeisen process rapidly decreases vapor pressure down toward ice saturation, thus eliminating water supersaturation. This is why we do not see supersaturation w.r.t. water in the requested Fig. 1.

Specific comments

- *Figure B1: please add a scale and orientation to this map!*
- The figure was updated, see Fig. 2

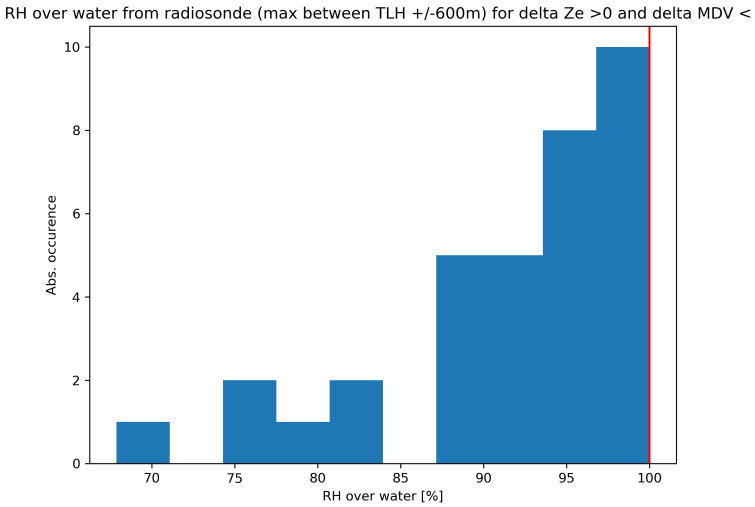

Figure 1. Max. relative humidity over ice inside TLH +/- 600 m where ΔZ_e >0 and ΔMDV <0.

- *Question about attenuation and new sentence on l.192 (and section 2.1.2): please clarify what you did for attenuation correction at 94 GHz! If you correct for gaseous attenuation at 35 GHz, you should do it at 94 GHz...*
- We agree, but since we do not use LIMRAD94 Ze we saw no need to describe the attenuation of LIMRAD94 Ze here. We only use Ze from the 35 GHz radar for the analysis of the Ze gradient. LIMRAD94 is only used for polarimetry which is not affected by gaseous attenuation.
- *Question about temperature inversion at Gothic Mountain top height: I did not understand the response involving subsidence, could you please clarify/elaborate?*
- With entrainment we ment the mixing of dry air into the cloud layer by turbulence. However, due to the concerns of Reviewer 2, the case study on Feb 21, 2023 was removed.
- *Figure 5: if you consider that this is a standard plot and that all ACP readership is familiar with it, then why defining the curves corresponding to temperature, dew point temperature, wind barbs, and not the others curves (lapse rates, mixing ratio...)? I would suggest to define all curves displayed in the plot.*
- We agree, however due to the concerns of Reviewer 2, the case study on Feb 21, 2023 was removed and hence also the Fig. 5
- *Question about kinetic energy and number of splinters: please add the explanation and the reference at this location of the main the text.*

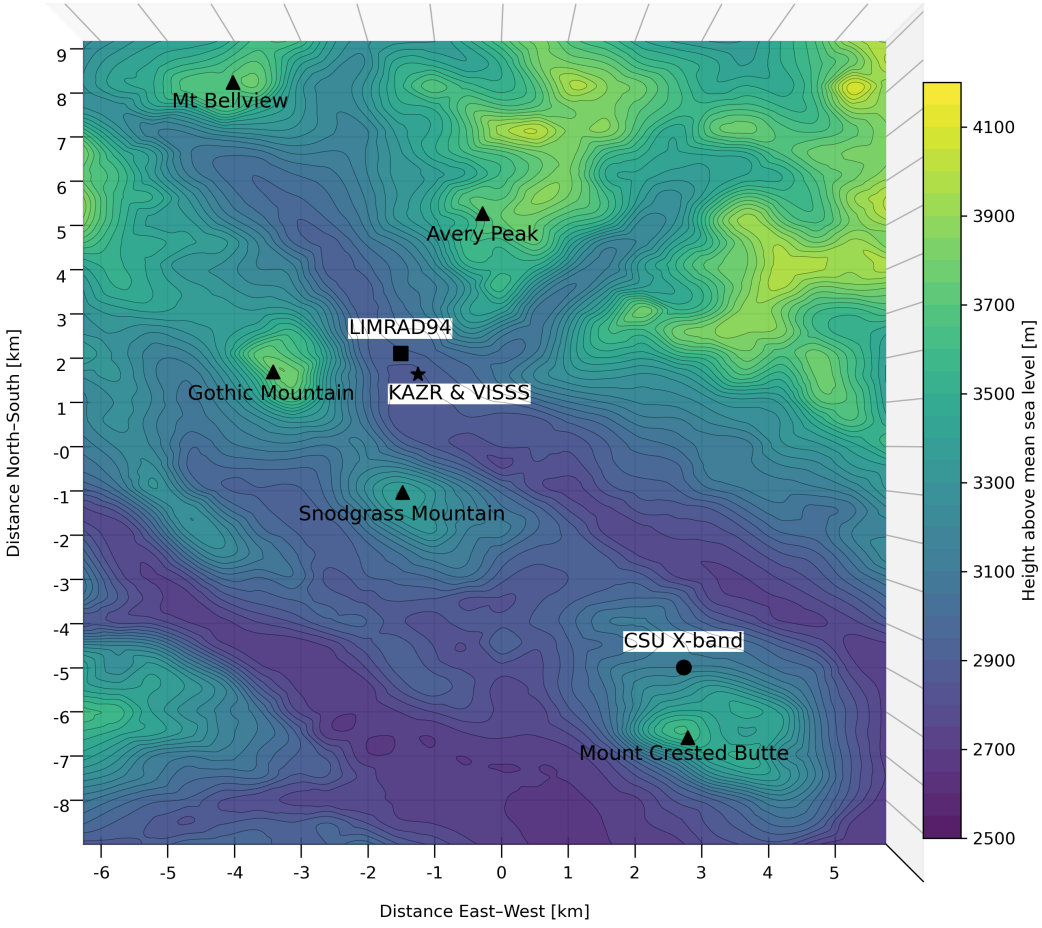

Figure 2. Elevation plot of the measurement site with all relevant mountain peaks and instrument locations marked.

– We added the following sentence:

L414f.:

They also showed that the number of splinters increased with increasing collision kinetic energy, which depends on both the particle masses and the square of their relative velocity.

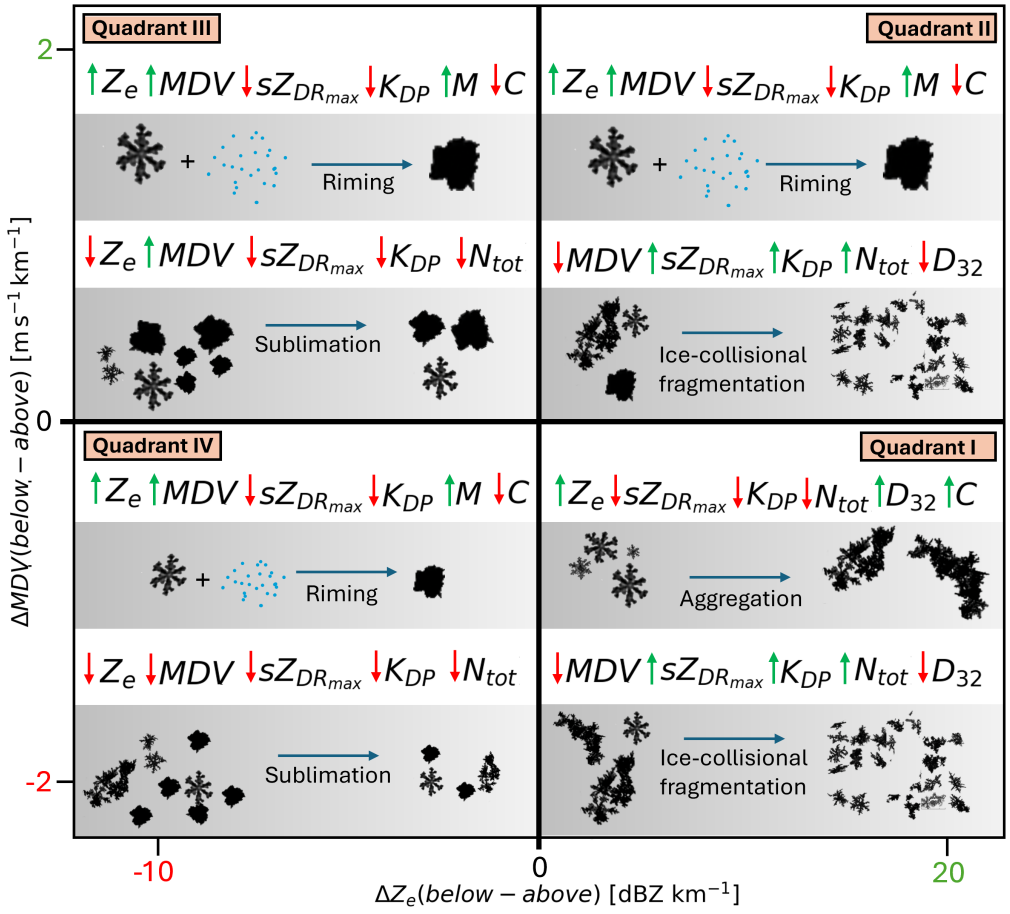

Figure 3. Conceptual diagram of the suspected (dominant) microphysical processes inside the turbulent layer, displayed similar to the four quadrants in Fig. 11. The impact of microphysical processes on radar and VISSS variables is also displayed qualitatively: Red downward facing arrows indicate a decrease of the respective variable, upward facing green arrows an increase. Note that for the radar variables (Z_e, MDV, $sZ_{DR_{max}}$ and K_{DP}), we can measure the change inside the turbulent layer. VISSS variables (N_{tot}, C, D_{32}, M) are measured below the turbulent layer. Their change due to the microphysical process is suspected based on the change of particle and PSD properties. If a variable is not depicted, no clear trend can be derived. The particle images were recorded by VISSS.

References

Author's response to:
RC#2
https://doi.org/10.5194/egusphere-2025-4517-RC2

Anton Kötsche[1], Maximilian Maahn[1], Veronika Ettrichrätz[1], and Heike Kalesse-Los[1]

[1]Leipzig Institute for Meteorology (LIM), Leipzig University, Leipzig, Germany

Correspondence: anton.koetsche@uni-leipzig.de

Summary of main changes of the manuscript:

- Added rationale to the empirical δ retrieval in Section 2.1.2 Polarimetric radar data, since our approach to removing δ from KDP is not published in another study (to our knowledge there is no other literature available that discusses the removal of δ in snow at W-band). We provide some plots of cases with δ for the reviewer to evaluate the δ removal method.
- Added new section (2.6 The turbulent layer) to explain turbulent layer formation behind Gothic Mountain based on a representative case study, since a more detailed description of the formation mechanism was requested by reviewer 2.
- Removed Sect 3.1 Case Study on February 21, 2023 because of the concerns of reviewer 2 regarding the influence of SIP not related to the turbulent layer and the close proximity of the cloud top to the turbulent layer, resulting in increased influence of INP.
- Small changes in the schematic figure requested by reviewer 1 (Fig. 11 in new manuscript)
- Improvement of the map in the appendix based on remarks by reviewer 1 (B1)

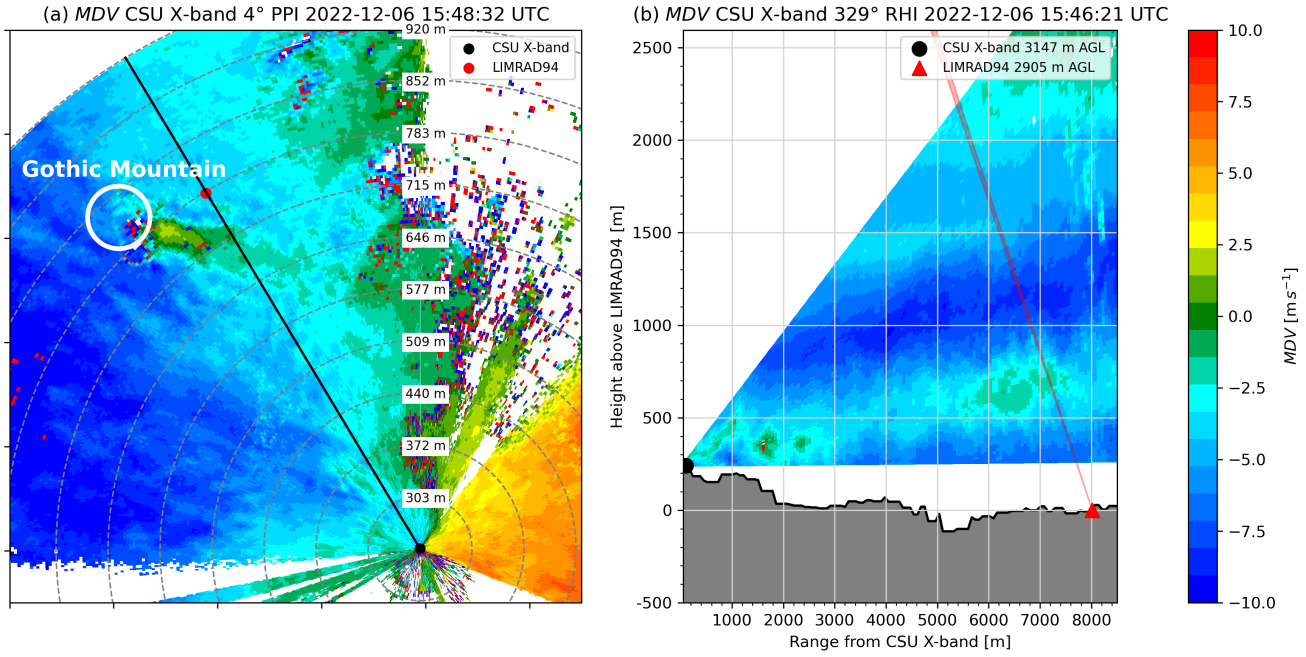

Figure 1. This figure was already presented in our previous study Kötsche et al. (2025), we show it again to visualize Gothic Mountain as main reason for the formation of the observed turbulent layer. a) Mean Doppler velocity (approx. radial component of horizontal wind) of CSU X-band PPI scan at 4 ° elevation angle with location of Gothic Mountain (white circle) and direction of RHI scan at azimuth 329 ° (black line) at 15:48:32 UTC on Dec 6, 2022. The map is displayed in a north-up orientation, with north at the top of the figure. Grey dashed circles are placed at every 1000 m range from CSU X-band. Labels are the respective heights above LIMRAD94 of the CSU X-band radar beam. b) Mean Doppler velocity of CSU X-band RHI scan (azimuth 329 °) at 15:46:21 UTC on Dec 6, 2022 with LIMRAD94 beam direction (red). Grey shading shows the elevation profile.

Response to RC#2:

- *Computation of KDP. It is good that you are aware of the δ impact now. I understand that you simply removed the potential contaminated cases, since improving KDP computation is way too much for this paper. However, it appears to me that the used method for excluding δ lacks theoretical or practical support. If you are following some established approaches, literature should be given.*

- The retrieval and its thresholds were chosen based on cases in our data where backscatter was observed. We acknowledge that the thresholds are empirical, but to our knowledge there is no other literature available that discusses the removal of δ in snow at W-band. The approach described in Myagkov et al. (2020) using Doppler spectra in low turbulence conditions and during rain is obviously not applicable in our case. Also in other studies using KDP at W-band (e.g. Von Terzi et al. (2022)) no description of δ removal was provided. We provide plots of the main cases including backscatter differential

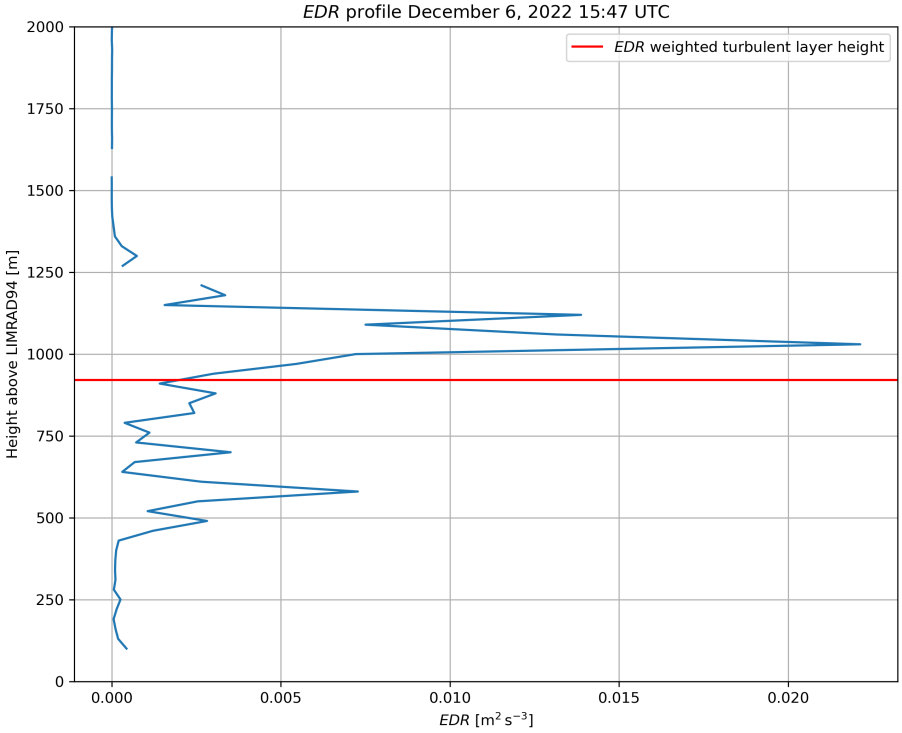

Figure 2. EDR profile (blue) and EDR weighted TLH as described in Sect. 2.6.1 in on Dec 6, 2022 15:47 UTC, approximately the same time the radar scans of CSU X-band in Fig. 1 were performed.

phase (see Fig. 3-6) so the reviewer may evaluate the performance of the δ removal. We also added the following clarifying statement with the description of our δ removal method.

L121f.:

We acknowledge that the thresholds selected for the removal of δ are empirical and based on observations from instances where we noted the contribution of backscatter differential phase in our data. The method enables us to drop the majority of δ contaminated data, but the thresholds may not be directly applicable to other radar data. To the authors knowledge, there is currently no other literature available that addresses the removal of δ in snow at W-band. The approach described in Myagkov et al. (2020), which utilizes Doppler spectra in low turbulence conditions and was demonstrated during rain is not applicable in our case. It would be desirable for future publications to develop a solid method to remove the δ contribution from Φ_{DP} directly, before calculating KDP.

– *Computation of EDR. I am not familiar with the Vogl 2024 approach. Looking at your new Fig. 3b, I would say that your calculations could be biased to small values. For this turbulent case, EDR should be decently large and presents large variations. Unfortunately, I do not see that from your plot.*

– The computation of EDR follows a known approach originating from Borque et al. (2016). It was used in multiple publications including Vogl et al. (2022, 2024) where the thresholds for turbulence used in this paper were derived. We also frequently see EDR values exceeding $1\,\mathrm{m}^2\,\mathrm{s}^{-3}$ in strong turbulence. We added an additional remark to the original paper in section 2.5 Turbulence eddy dissipation rate retrieval.

– *Attribution of the turbulent layer formation. I am not convinced by the randomly listed evidence. They are poorly supported to me, and could be quite misleading to the ACP readers. Since the focus of this work is the impact of this turbulence layer, you need to clearly discuss where and how this layer is formed. At the very least, you should clearly say that this is your assumption in all relevant places and carefully discuss potential responsible factors. Of course, the evidence linked to your assumptions should be given as well.*

– We understand the reviewers concern on the formation machanism of the turbulence layer and hence added the following exemplary case study in the paper to strengthen our argumentation and show the formation mechanism of the turbulent layer. We also added a small section on the CSU X-band radar used for the scans.

L184f.:

Due to the orography surrounding the measurement site, we observed a distinct layer of enhanced turbulence, predominantly at and below 1000 m above ground level (AGL). Gothic Mountain, a cone-shaped mountain located just west of the measurement site (see Fig. B1), is suspected to be the primary driver for the formation of this turbulent layer. To illustrate this, we will present an exemplary case study on Dec 6, 2022 where the formation mechanism of the turbulent layer is visible. This case study was previously described in (Kötsche et al., 2025). Fig. 1 shows the MDV of CSU X-band from a PPI (a) and a RHI (b) scan at around 15:48 UTC and 15:46 UTC, respectively. During that time, EDR indicates enhanced turbulence between 500 and 1200 m AGL, with the mean EDR weighted turbulent layer at 900-950 m (Fig. 2). The MDV observed in the PPI scan can be interpreted as the radial component of the horizontal wind. Negative values (blue) in Fig. 1 represent motion toward the radar, while positive values (yellow–red) indicate motion away from it. Although parts of the PPI are blocked by surrounding mountains, a prevailing westerly flow is evident from the blue shading west of the CSU X-band and the orange–red shading to the east. Where MDV approaches zero, the wind direction is nearly perpendicular to the radar beam. Downstream of Gothic Mountain, a narrow band appears in which MDV abruptly changes sign to positive, contrasting sharply with the surrounding negative values. This pattern indicates that, in the lee of Gothic Mountain, the wind veers toward a more southerly direction, though this effect weakens rapidly further downstream. In the RHI scan (Fig. 1b), this southerly component is expressed as a region with predominantly green colors at ranges of 6000–7000 m from the CSU X-band and altitudes of 500–900 m above LIMRAD94. This disturbance may be partly associated with a counterflow, suggesting blocked low-level flow, similar to the situations discussed in Ramelli et al. (2021). Enhanced wind shear develops along the upper and lower boundaries of this counterflow, likely producing the turbulence identified by EDR in Fig. 2. The two peaks in EDR are well collocated with the upper and lower edges of the counterflow. The LIMRAD94 beam is depicted as a red cone in Fig. 1b), clearly showing that LIMRAD94 measurements are influenced by this turbulence. This wind pattern is frequently observed behind Gothic Mountain, although the location of the counterflow and hence the height of the turbulent layer depends on the wind direction (see Fig. 7). We therefore argue that Gothic Mountain is the main driver for the observed turbulence at the measurement site.

L100f.:

Also, a scanning dual polarization X-band radar (CSU X-band) from Colorado State University (CSU) was deployed in a distance of 8018 m (at 149 ° azimuth and 3147 m AMSL) from LIMRAD94 (also see Appendix, Fig. B1). From the CSU X-band radar data, RHI scans at 329 ° azimuth (towards the AMF2 and LIMRAD94) and plane position indicator (PPI) scans at 4 ° elevation were used in Fig. 1.

– *Consideration of shallow precipitation cases. I disagree. Your discussion on INP does not support the inclusion of shallow precipitation events. It is widely observed that Ninp can be much smaller than the observed Nice, and one of the*

explanations is SIP. A representative case showing that Nice is amplified by 100 folds near the cloud top is given in Fig. 5 of (Luke et al., 2021). Hence, cloud top generating cells can simply explain SIP, and your turbulence story is obviously personally biased.

– *We acknowledge that the case study may not contribute to the overall understanding of microphysical processes in the turbulent layer due to the concerns mentioned by the reviewer. We therefore chose to remove the case study, as it is not significantly contributing to the main scope of the paper.*

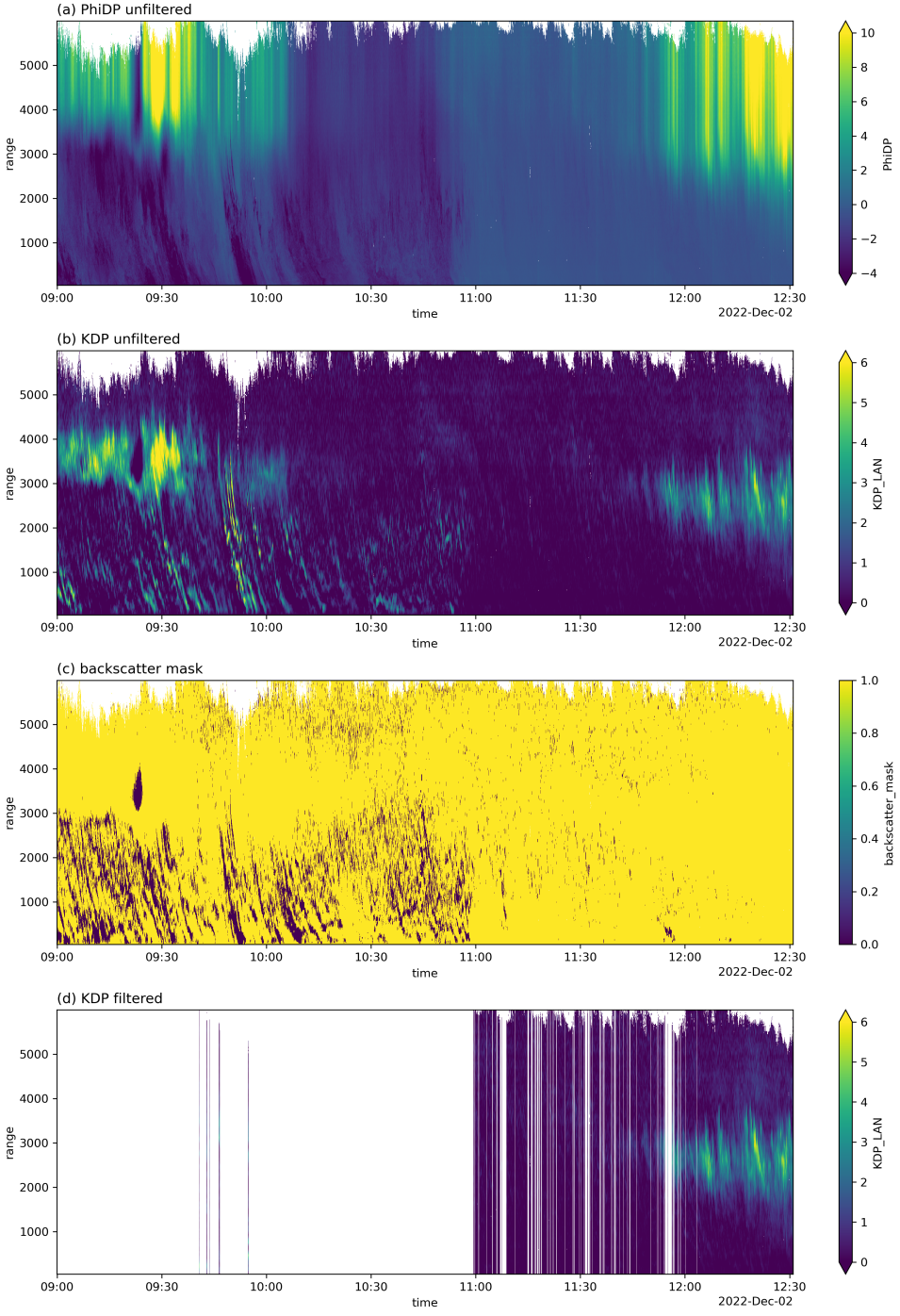

Figure 3. Case study on Dec 2, 2022: (a) unfiltered PhiDP, (b) unfiltered KDP, (c) backscatter mask (0 where backscatter is detected), (d) KDP filtered based on backscatter mask.

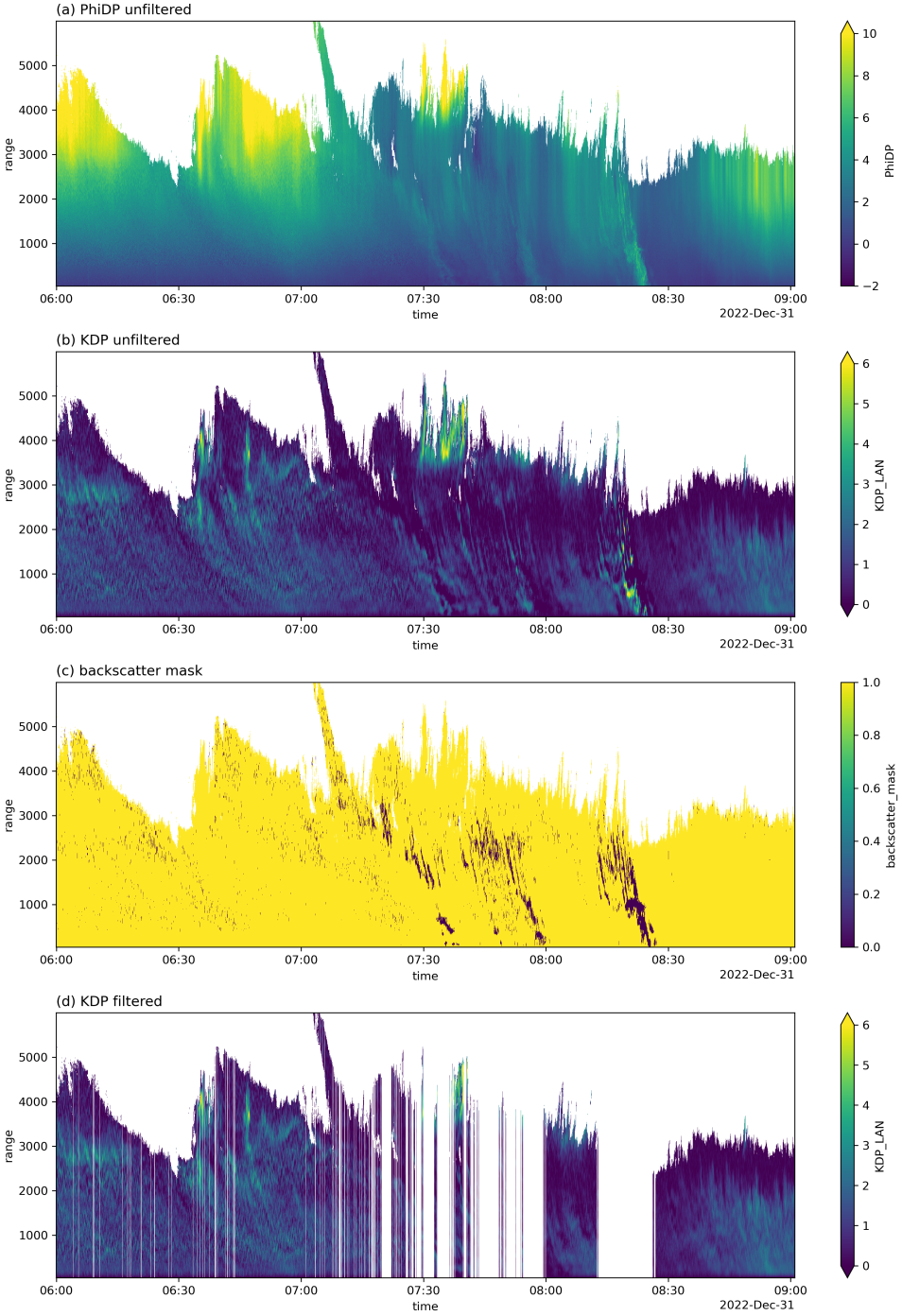

Figure 4. Case study on Dec 31, 2022: Descriptions as in Fig. 3

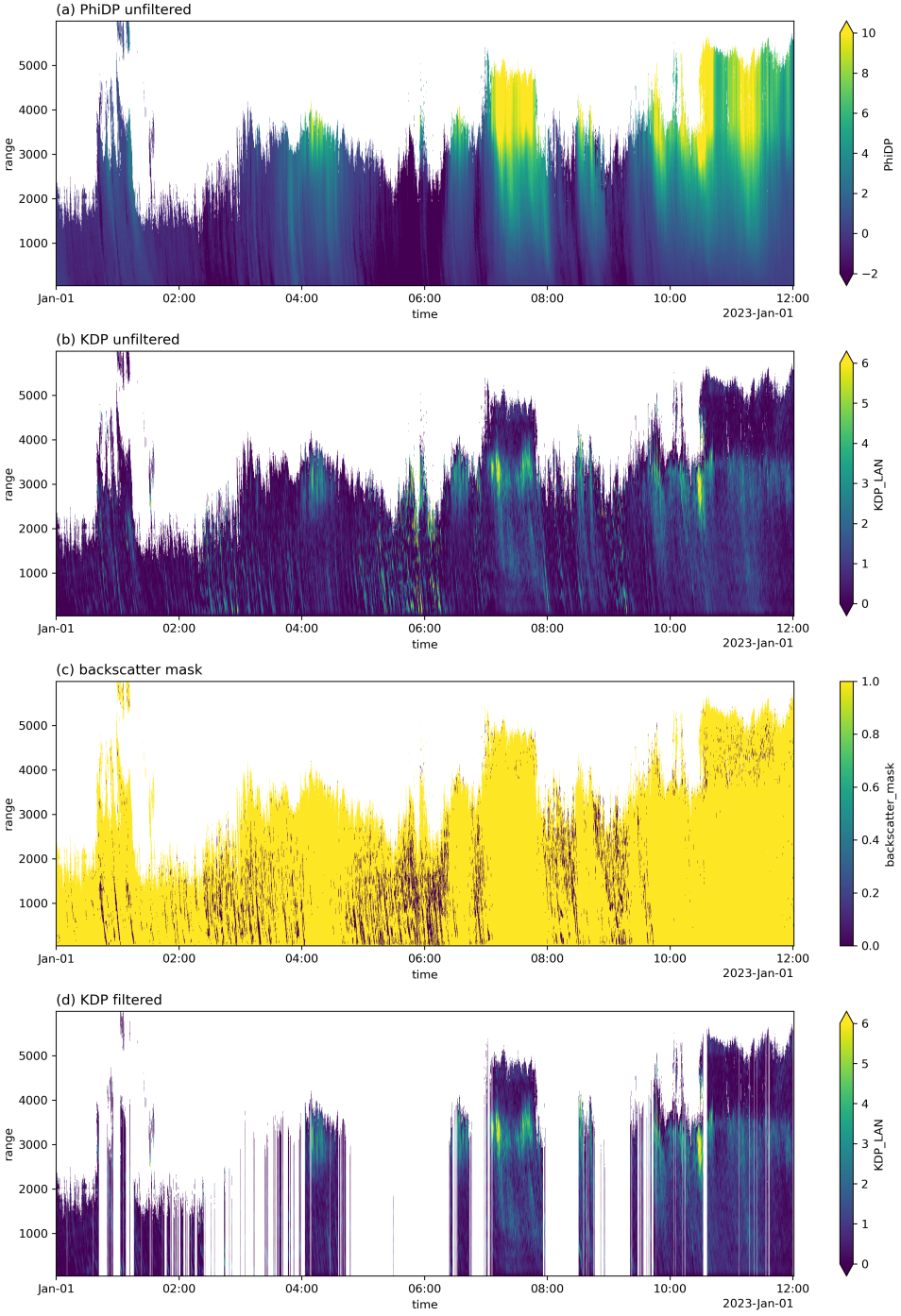

Figure 5. Case study on Jan 1, 2023: Descriptions as in Fig. 3

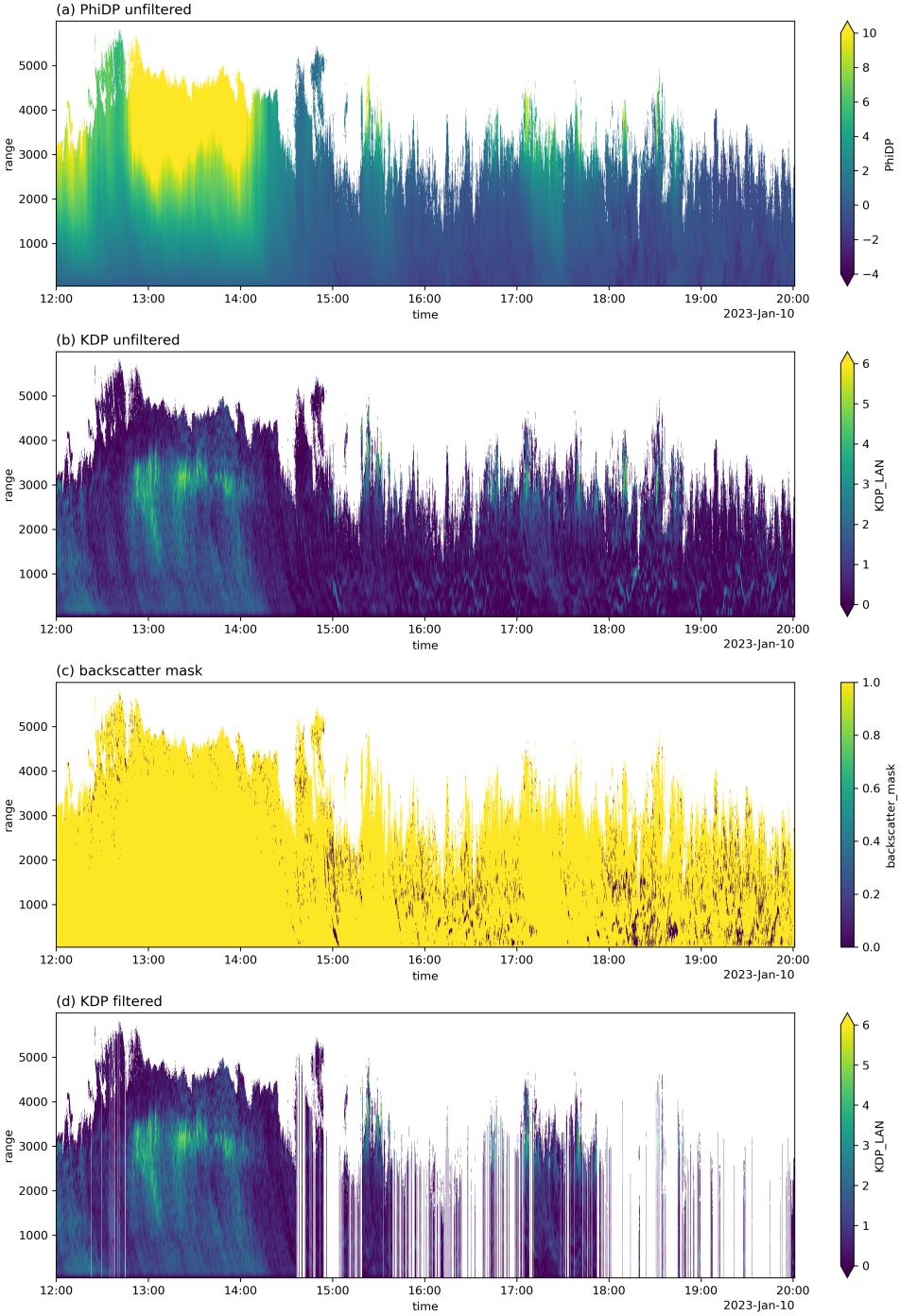

Figure 6. Case study on Jan 10, 2023: Descriptions as in Fig. 3

References

Borque, P., Luke, E., and Kollias, P.: On the unified estimation of turbulence eddy dissipation rate using Doppler cloud radars and lidars, Journal of Geophysical Research: Atmospheres, 121, 5972–5989, https://doi.org/10.1002/2015JD024543, 2016.

Kötsche, A., Myagkov, A., von Terzi, L., Maahn, M., Ettrichrätz, V., Vogl, T., Ryzhkov, A., Bukovcic, P., Ori, D., and Kalesse-Los, H.: Investigating KDP signatures inside and below the dendritic growth layer with W-band Doppler Radar and in situ snowfall camera, EGUsphere, pp. 1–38, https://doi.org/10.5194/egusphere-2025-734, 2025.

Myagkov, A., Kneifel, S., and Rose, T.: Evaluation of the reflectivity calibration of W-band radars based on observations in rain, Atmospheric Measurement Techniques, 13, 5799–5825, https://doi.org/10.5194/amt-13-5799-2020, 2020.

Ramelli, F., Henneberger, J., David, R. O., Lauber, A., Pasquier, J. T., Wieder, J., Bühl, J., Seifert, P., Engelmann, R., and Hervo, M.: Influence of low-level blocking and turbulence on the microphysics of a mixed-phase cloud in an inner-Alpine valley, Atmospheric Chemistry and Physics, 21, 5151–5172, https://acp.copernicus.org/articles/21/5151/2021/, 2021.

Vogl, T., Maahn, M., Kneifel, S., Schimmel, W., Moisseev, D., and Kalesse-Los, H.: Using artificial neural networks to predict riming from Doppler cloud radar observations, Atmospheric Measurement Techniques, 15, 365–381, https://doi.org/10.5194/amt-15-365-2022, 2022.

Vogl, T., Radenz, M., Ramelli, F., Gierens, R., and Kalesse-Los, H.: PEAKO and peakTree: tools for detecting and interpreting peaks in cloud radar Doppler spectra – capabilities and limitations, Atmospheric Measurement Techniques, 17, 6547–6568, https://doi.org/10.5194/amt-17-6547-2024, 2024.

Von Terzi, L., Dias Neto, J., Ori, D., Myagkov, A., and Kneifel, S.: Ice microphysical processes in the dendritic growth layer: a statistical analysis combining multi-frequency and polarimetric Doppler cloud radar observations, Atmospheric Chemistry and Physics, 22, 11 795–11 821, https://acp.copernicus.org/articles/22/11795/2022/acp-22-11795-2022.html, 2022.